Dieudonné Kabombo, Dariush Azizi, Réjean Hébert and Faïçal Larachi*

Multistep concentration of lizardite/antigorite from chrysotile mine tailings – case of the Carey Mine site in East-Broughton (Québec)

https://doi.org/10.1515/ijcre-2020-0242
Received December 18, 2020; accepted March 14, 2021;
published online March 25, 2021

Abstract: Revalorization of mining residues is of central concerns to the mining industry and the environment. Specifically, environmental management of residual products from the exploitation of chrysotile in the Thetford Mines region is one of the government concerns in Quebec and Canada. This work uses mining wastes in a second resource generation for production of magnesium from cheap and health-friendly mineral sources; the goal being to produce chrysotile-depleted pre-concentrates for a use as precursors in the leach off extraction of magnesium. The concentration of lizardite/antigorite from chrysotile containing serpentine rock mine tailings originating from the Carey Mine site in East-Broughton (Québec) was carried out using a suite of hydrocyclone, settling/decantation and magnetic separations. Four size classes of the mining residue, namely (−3150,+1580), (−1580, +600), (−600, +300) and (−300, +150) μm, were tested with an aim to reduce the level of objectionable asbestos fibers to allow access to the safer Mg-bearing minerals contained in the mine waste sources. The asbestos fibers clean-up consisted of subjecting the sieved fractions to two hydrocyclone steps, six settling/decantation steps and two magnetic separation steps. The best results were achieved when the hydrocyclone separators led to Mg recovery of 85% (±4) for the coarsest size fraction size. Both hydrocyclone underflow streams underwent settling/decantation separations. The settling tests lasted 30 min and led to Mg recoveries of 82.5% (±1.8) of Mg in the ultimate concentrate. SEM characterizations revealed that it was possible to reduce substantially the amount of chrysotile fibers to render the coarse-sized fraction in the mining waste usable while significantly lowering the health risk of the fibers. A two-step magnetic separation was applied to the final settling/decantation underflow to remove magnetic minerals such as magnetite from the lizardite/antigorite concentrate. The final quasi-non-magnetic chrysotile-depleted lizardite/antigorite concentrate allowed sample recovery of 62.5% (±0.9) wt. of Mg. These preliminary results are intended as a first compulsory step in support of viable restoration and sustainable development scenarios for the Thetford Mines mining sites as second-breath sources for valuable magnesium.

Keywords: antigorite; lizardite; mining residue; physical separation; serpentine; waste valorization.

1 Introduction

The exploitation of chrysotile asbestos had to come to a halt in 2012 after over a century of industrial mining activity following the causal link established between asbestos fibers and occupational health issues for the field workers chronically exposed to raw/manufactured chrysotile products (Nicholson 2001). Nonetheless, the mineral extraction since the 1880s had led to an accumulation of large amounts of wastes in the form of chrysotile mine tailing piles. These artificial man-made aboveground “inverted” mines have become an appealing source for minerals, as a rich source of magnesium (Barbeau, Couture, and Roy 1972; Thibault 2011), in demand by modern industrial activities. Unlike the fibrous chrysotile present in minor proportions, lizardite and antigorite are the two most abundant sheet-like polymorphs in chrysotile mine tailings. Obviously, revalorization of mining residues has become central to the mining industry and the environment due to the green opportunity they offer by allowing the supply of key metals and/or

***Corresponding author: Faïçal Larachi**, Department of Chemical Engineering, Laval University, 1065, Avenue de la Médecine, Québec City, QC G1V 0A6, Canada, E-mail: faical.larachi@gch.ulaval.ca
Dieudonné Kabombo, Department of Chemical Engineering, Laval University, 1065, Avenue de la Médecine, Québec City, QC G1V 0A6, Canada; and Centre de Technologie Minérale et de Plasturgie, 671, Boulevard Frontenac Ouest, Thetford-Mines, QC G6G 1N1, Canada
Dariush Azizi, Department of Chemical Engineering, Laval University, 1065, Avenue de la Médecine, Québec City, QC G1V 0A6, Canada; and Institut National de la Recherche Scientifique (INRS-Eau Terre et Environnement), Université du Québec, 490 Rue de la Couronne, Québec City, QC G1K 9A9, Canada
Réjean Hébert, Centre de Technologie Minérale et de Plasturgie, 671, Boulevard Frontenac Ouest, Thetford-Mines, QC G6G 1N1, Canada; and Department of Geology and Geological Engineering, Laval University, 1065, Avenue de la Médecine, Québec City, QC G1V 0A6, Canada

minerals. Likewise, it can cause significant reduction in greenhouse gas emission and infrastructure investments for costly mining technologies.

Magnesium in its metallic form has found applications in the industry due to its notable characteristics in terms of material rigidity, light weight and wear resistance. In the form of mineral oxides, oxy-hydroxides or silicates, magnesium is also used in the chemical and biological industries for the production of chemical fertilizers, salt for road, use in health industry, etc (Blazy 1970). The most popular application of Mg-bearing mine tailings as cheap alkaline sources for the capture of anthropogenic carbon dioxide acidic emissions has been in the air for many years. However, industrial production of Mg from serpentine rock tailings faced resistance such as with the Magnola process which never took off 20 years ago (Huot and Hébert 2003). The main objection to the use of chrysotile mining tailings concerns non-compliance with the standards to abide by that are associated with public health (Nicholson 2001). Numerous research studies have been conducted to find suitable methods to extract magnesium from tails. Specifically, studies have been carried out on the valorization of serpentine rock mine tailings by concentrating chrysotile and antigorite using physical separation techniques such as hydrocyclone, spiral concentrators and shaking tables (Barbeau, Couture, and Roy 1972; Blazy 1970; Collings 1977; Hébert 1985; Huot and Hébert 2003; Martinez 1974; Riordon 1973; Thibault 2011). Performance of gravity separators directly depends on their operating conditions and solids physical properties, optimization of these latter is essential to an efficient separation (Plitt, Flintoff, and Stuffco 1987). For instance, increasing the solids concentration in the pulp (Neesse et al. 2004) or increasing the pulp flow rate (Mukherjee et al. 2003) induces opposite trends on the particle size cut-off and thus on the process efficiency. Among these physical beneficiation methods, hydrocyclone separation has been identified as the most efficient process used in the chrysotile mining industry (Barbeau, Couture, and Roy 1972; Blazy 1970; Collings 1977; Hébert 1985; Huot and Hébert 2003; Martinez 1974; Riordon 1973; Thibault 2011). Throughout mineral separation in hydrocyclone, the mineral particles, being pulped, are separated through an acting centrifugal force by developing a negative pressure vortex along the hydrocyclone axis. In this condition, the less dense (or fibrous) particles will go towards an overflow (i.e., enriched in chrysotile) while the denser/coarser particles are routed towards an underflow (i.e., enriched in lizardite and antigorite) (Collings 1977). In addition to gravity separators, the use of magnetic separators has been attempted to beneficiate lizardite and antigorite and their separation from ferromagnetic bearing minerals (e.g., magnetite) (Sztuke 1979; Veetil et al. 2015).

The subject of this study is to develop a concentration process for recovering lizardite/antigorite from chrysotile contained in the serpentine rock mine tailings originating from the Carey Mine site in East-Broughton (Québec). Such an aim to commodify purified Mg *solid* sources, i.e., mainly lizardite and antigorite, will allow commercial exploitation of this waste-resource by downstream industrial actors in needs to procure a safe Mg *mineral* source for their own industrial operations without necessitating additional investments to comply with the regulations *vis-à-vis* the obnoxious nature of the chrysotile fibers. If such a goal admits disruption of the raw mine tailings, it renders solid streams commercially available with minimized fibers' content in the commodified solid streams. We present in this study the first phase of research on the beneficiation of lizardite and antigorite as Mg-bearing serpentine silicate minerals as potential precursors to chemical or biological leaching (Riordon 1973) after tailings clean-up of its chrysotile fiber content. Matter-of-factly, lizardite and antigorite are characterized by their less dissolution kinetics under acidic conditions as compared to chrysotile (Evans 2010; Viti et al. 2018). However, apart from these magnesium silicate polymorphs, chrysotile mine tailings also contain other mineral components, mainly magnetite from the hydration of olivine (Huot and Hébert 2003), talc from the alteration of orthopyroxene, and magnesite from the ambient mineral carbonation of erstwhile brucite or serpentines.

In this study, the main mineralogical, chemical and physical characterizations of the Carey mine tailings were completed. Then, a laboratory-based experimental protocol consisting of several physical separation steps was carried out using a suite of hydrocyclone, settling/decantation and magnetic separations. Evidence of chrysotile removal was elaborated on the basis of thorough scanning electron microscopy (SEM) observations. Finally, the separation-concentration best conditions were evaluated through comparisons of Mg recoveries as well as Si/Mg and Fe/Si ratios of the separation products with an aim to produce chrysotile-depleted final non-magnetic underflow concentrate rich in lizardite/antigorite.

2 Material and methods

2.1 Minerals and characterization methods

Samples of mining serpentine rock residue with a total mass of 120 kg were collected at 1 m depth from five different spots located on the sides of the waste pile from the former Carey Mine site (Canadian Inc., East-Broughton, Québec). The samples were stored in five 20 L capacity

polyethylene containers at room temperature for subsequent tests and analyses.

The particle size distribution of the samples was determined by coarse sieving with a SWECO type Vibro-Energy round separator having steel meshes within the [3150–150] µm range. Four size classes, namely (–3150, +1580), (–1580, +600), (–600, +300) and (–300, +150) µm were isolated with the respective percent yields, 22, 32, 24 and 22%. The choice of these four fraction sizes was made according to the overflow and underflow openings of the hydrocyclone used for the concentration of lizardite and antigorite in this investigation. To simplify notations, only the values of upper mesh will be used to identify these size classes in the rest of text: (+1580), (+600), (+300) and (+150) µm.

The residue sample mineralogy was identified by X-ray diffraction (XRD) using a portable Inxitu Terra 237 diffractometer with Co Kα radiation by sweeping the 2θ diffraction angle over a range of 5–55° at 0.02°/s (Viti et al. 2018). A SEM equipped with an energy dispersive X-ray detector (Hitachi [SU1510] & Bruker [Quantax]) was used for powder samples' semi-quantitative analyses. Raman scattering spectroscopy (Bruker Senterra & Olympus BX51) was used to identify characteristic signatures from the different serpentine polymorphs in the analyzed powder samples. The specific surface areas of the samples were determined by means of a Micromeritics analyzer (Gemini VII – Model 2390t) whereas their relative density was measured using a helium pycnometer (Micrometritics accupyc ii1340). The total carbon analysis of the as-received residue was performed on a Leco apparatus whose analytical limit is 0.01%. The mass of sample taken for analysis, *ca.* 2 mg, was inserted in a nacelle to which vanadium pentoxide was added as oxidant.

Analysis major elements of the samples was performed in X-ray fluorescence (XRF) using a Bruker-type dispersion spectrometer (S8 Tiger). Analysis was carried out on melted-borated samples following loss on ignition at 1000 °C in pressed pellets. The elemental concentration is detectable in ppm with an accuracy of about 0.05%. The SEMIQUANT software was used for quantification of major and minor oxides in terms of recovery and grade in the solid samples before and after separation. In particular, the oxide mass contents (%) were subsequently converted to elemental grade (%) for determination of Si/Mg and Fe/Si concentration ratios both in the initial sieved samples and in their separated concentrate or rejection products. The Si/Mg ratio was chosen as the main indicator of the separation efficiency to recognize the serpentine polymorphs. According to O'Hanley (Fouquet et al. 1997), Si/Mg ≈ 0.67 reflects leaflet morphologies reminiscent of lizardite whereas Si/Mg ≈ 0.78 leans rather towards the fibrous chrysotile (Büttner and Saager 1982). Iron as the main contamination in the serpentine rock residue after separation was assessed through the Fe/Si ratio.

2.2 Separation-concentration experiment protocol

General scheme of the physical separation steps of the serpentine rock tailings from the East-Broughton mine waste pile is illustrated in Figure 1 for which three separation-concentration (physical separators) methods were used to treat 4 kg batches of each of the four size fractions of the mining residues.

In the first step, 4 kg of sieved samples were pulped for 5 min under agitation at 1725 rpm in a reservoir prior to be fed into a 2″ ID Krebs hydrocyclone using a diaphragm pump capable of delivering pulp feed rates between 22 and 36 L/min at pressures from 4 to 10.5 psi (Figure 1). The feed pressure was maintained for all tests at 8.5 psi corresponding to a flow rate of 32 L/min for four sieved fractions pulped at 30, 40 and 50% solids loadings. For each combination of sieved fraction and pulp concentration, the underflow stream, UFH-1, from first separation was re-pulped before undergoing a second hydrocyclone separation to yield a chrysotile-depleted lizardite/antigorite concentrate in the form of an

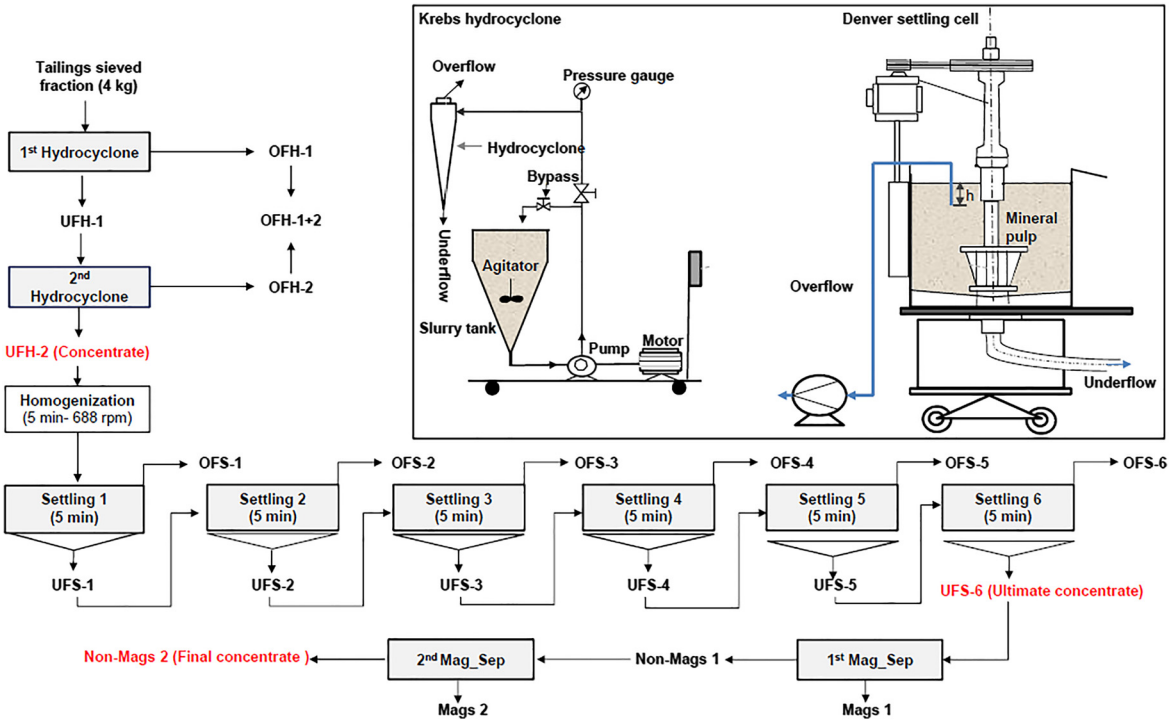

Figure 1: General protocol used for the separation-concentration experiments undertaken for beneficiation of the mining residue.

underflow stream UFH-2 (Figure 1). In this manner, OFH-1 and OFH-2 overflow streams from hydrocyclone separation (Figure 1) enabled retention of some of the fines and chrysotile fibers contained in the treated feeds. Both overflow streams were subsequently mixed into one single chrysotile-rich overflow stream. For all tested separation modalities, the products of (overflow/underflow) separation were filtered, dried in an oven at 100 °C for 24 h, and weighed before characterization and analysis. The separation efficiency was evaluated on the basis of product quality, i.e., as Mg, Si and Fe recoveries and in terms of Si/Mg and Fe/Si ratios of the hydrocyclone products.

In a second step, settling tests were performed on the final hydrocyclone concentrate (UFH-2) using a 70-L capacity Denver cell to further polish removal of the recalcitrant chrysotile fibers and fine particles that might have sneaked into the hydrocyclone concentrate. Approximately 3 kg of hydrocyclone concentrate were pulped in *ca.* 47 L water to achieve relatively dilute pulps with *ca.* 5% solids concentration. After stirring for homogenization during 5 min at 688 rpm, the pulp was allowed to decant for 5 min. During this time interval, a Masterflex *P/S 1400 Series Laboratory peristaltic pump with a suction flow rate of 100 mL/min was used to collect the objectionable jetsam of chrysotile fibers and fine particles in the overflow stream (OFS-1). For each of the particle size fraction used (+1580, +600, +300 and +150 microns) in this study, the solid concentration was maintained at 5 wt% and the stirring speed at 688 rpm. The overflow suction rate was set at 100 mL/min for 30 min for all of the tests. A six-fold depletion sequence of the solids suspension to be cleansed was scheduled as illustrated in Figure 1. Each time, the overflow liquid collecting the entrained jetsam (OFS-1–OFS-6) was enabled after 5 min of decantation time of the Denver cell. Likewise, underflow sampling and re-pulping (UFS-1–UFS-5) has been planned to withdraw samples under gravity underflow at the opening of the bottom valve (Figure 1). After sixth settling/decantation operations, the ultimate concentrate (UFS-6) accumulated at the bottom of the cell was recovered by gravity at the opening of the drain valve. The products resulting from the separation were filtered, dried at 100 °C for 24 h prior to their characterization. The efficiency of separation was evaluated in terms of kinetic curves as a function of the settling time along with the evolution of the Si/Mg in the separation products.

As a third and final step, magnetic separation was carried out on the ultimate concentrates (UFS-6) to get rid of their ferromagnetic mineral content, mainly magnetite. Typically, 1 kg of dried concentrate samples was exposed to two sweeps by a permanent magnet (SEPOR type, GENEQ Inc.) with a magnetic field intensity of *ca.* 700 Gauß. The magnet device consisted of an aluminum assembly with a magnetic iron ball attached to a rod. Upon actuation of the magnetic field, the rod enabled cherry-picking the magnetic minerals (Mags 1 & Mags 2) from UFS-6 concentrate to yield the final non-magnetic concentrate (Non-Mags 2), see Figure 1.

3 Results & discussion

3.1 Minerals characterization

The sieved fractions of the mine tailings were first characterized to disclose their physical, chemical and mineralogical properties as presented in Table 1. As presented in Table 1, in the case of particle size distributions, the coarsest fraction (+1580 µm) was the most abundant in the tailings as compared to the three finer ones which contributed almost equally. Regarding chemical properties of the sample, elemental analysis for the metals, and Si and C content revealed the presence (in order of mass percentage in the sample) of Mg, Si, Fe, C, Al, Cr, Ca, Na, Ni and K irrespective of sieved fraction (Table 1). Detection of *ca.* 1.5% C in the samples can be due to either presence of carbonatite minerals or to weathering products resulting from the "atmospheric" mineral carbonation of Mg and Ca bearing minerals pre-existing at the time of disposal in the ore mineralogy (Bodénan et al. 2014; Zarandi et al. 2017). For instance, the reaction over time of brucite and the serpentine rock with atmospheric CO_2 is sensitive to the prevailing ambient parameter variations such as temperature, CO_2 composition, water saturation, and seasonal wetting/drying and freeze/thaw cycles. Ambient carbonation leads to various hydrous magnesium carbonates, e.g., nesquehonite, and thus is certainly one of the main reasons behind detection of carbon C (Table 1) in our samples (Zarandi et al. 2017).

Table 1: Chemical, physical and mineralogical characteristics of the serpentine rock mining residue.

Element mass %	**Sieved fraction size (µm)**			
	(+1580)	**(+600)**	**(+300)**	**(+150)**
Mg	22.1	21.7	21.3	21.5
Si	17.7	16.8	15.9	16.0
Fe	5.15	6.36	7.09	7.47
C	0.81	1.22	1.51	1.57
Al	0.58	0.61	0.62	0.61
Cr	0.28	0.39	0.35	0.38
Ca	0.23	0.27	0.26	0.27
Na	0.12	0.09	0.09	0.22
Ni	0.14	0.20	0.17	0.22
K	0.07	0.10	0.10	0.1
Physical properties	**(+1580)**	**(+600)**	**(+300)**	**(+150)**
Specific surface area (m^2g^{-1})	7.6	14.5	15.8	16.7
Density (g cm^{-1})	2.61	2.81	2.9	2.9
Mass fraction (%)	31.9	24.1	22.1	21.9
XRD results-identified minerals[a]	**(+1580)**	**(+600)**	**(+300)**	**(+150)**
Lizardite/antigorite	M	M	M	M
Chrysotile	m	m	m	m
Hydromagnesite	m	m	m	m
Magnetite [$(Fe^{2+}Fe_2{}^{3+})\ O_4$]	m	m	m	m
Talc [$Mg_3(Si_2O_5)_2(OH)_2$]	m	m	m	m
Clinochlore [$(Mg, Fe^{2+})_5Al(Si_3Al)\ O_{10}(OH)_8$]	tr	tr	tr	tr
Biotite [$K(Mg,Fe^{2+})_3AlSi_3O_{10}(OH,F)_2$]	tr	tr	tr	tr
Element mass ratio (g/g)	**(+1580)**	**(+600)**	**(+300)**	**(+150)**
Si/Mg	0.80	0.77	0.75	0.74
Fe/Si	0.14	0.18	0.21	0.22
C/Mg	0.037	0.056	0.071	0.073

[a]M = major (10%); m = minor (1%); tr = trace (less than 1%).

Likewise, it was observed that the most abundant elements in the sample are Mg and Si which their concentrations are homogeneously detected in different size fractions. However, this evenness did not mask sensitivity of the Si/Mg ratio to particle size indicating a clearly decreasing trend from coarsest (Si/Mg = 0.80) to finest (Si/Mg = 0.74) fractions (Table 1). Depending on particle size, these ratios are also seen to deviate in an irregular manner with respect to the theoretical Si/Mg = 0.77 *mass* ratio for the contaminant-free serpentines ($Mg_3Si_2(OH)_4$). Lizardite, antigorite and chrysotile were identified through XRD as the prominent minerals in the sieved samples of the mine tailings (Table 1). However, traces of talc (Si/Mg = 1.54), biotite (Si/Mg = 1.16), and clinochlore (Si/Mg = 0.69) were also detected (Table 1) contributing to impact, by excess or default, the overall Si/Mg ratio with respect to the theoretical ratio. Worthy of notice is the fact that tremolite–actinolite fibers, as another type of asbestos, were not detected in the sample by XRD. Despite their attested presence in the Thetford Mines region mining tails (Case et al. 1997; Germine and Puffer 2015, 2020), it may be argued that their concentration level is below the XRD analytical detection limit. This would lead to the reasonable assumption that the chrysotile fibers are the main contaminant to cope with. A final important remark that should be regarded from an environmental standpoint, and also perhaps from the vantage point of another economic opportunity, is the presence of two transition metals, Ni and Cr, at meaningful concentration levels (Table 1) (Hamilton et al. 2018). From the latter perspective, nickel can eventually be aimed at from the sieved fractions. Indeed, nickel presumably in the sulfidic forms of pentlandite $(Fe,Ni)_9S_8$ and heazlewoodite (Ni_3S_2), or as nickel-iron alloys, e.g., awaruite ($Ni_{2.5\text{-}3}Fe$) is not uncommon in the serpentine lithologies such as in the Dumont sill project Abitibi-Temiscamingue region in North-Western Québec (Canada) (Zarandi et al. 2017). Amongst Ni and Cr, the latter element is of particular environmental concern, especially its toxic and carcinogenic hexavalent cation. Unlike the passive carbonation of mine tailings for which monitoring the escape of similar toxic metals through leaching into the receiving natural waters is compulsory (Hamilton et al. 2018), mature technologies already exist for the recovery/abatement of these metals from industrial streams before discharge.

Furthermore, carbon and iron contents gradually increased from the coarsest (+1580 μm) to the finest (+150 μm) fractions (Table 1). Doubling, on the one hand, of the carbon mass (from 0.037 to 0.073 g/g) on a per-gram basis of magnesium is evidence for greater carbonation reactivity with atmospheric carbon dioxide of the tailings as the sieved material gets finer (Table 1). On the other hand, the predominantly increasing trend of Fe/Si ratios the finer the particles points to the buildup of increasing amounts of iron-containing minerals, most notably magnetite [$(Fe^{2+}Fe_2^{3+})O_4$], and perhaps clinochlore and biotite, present as traces, according to XRD identifications (Table 1). However, a further complication in the interpretation of Si/Mg elemental ratios arises from the fact that Fe–Mg and Fe–Si intra-framework substitutions also occur both in octahedral and tetrahedral coordinations in the serpentines. Mössbauer spectroscopy analyses (Büttner and Saager 1982) in our group have shown that beside magnetite, the total intra-framework iron may account for up to 36% of the total iron present in the ore with up to 80% (20%) of the incorporated iron in octahedral (tetrahedral) coordination.

The XRD spectra corresponding to each sieved fraction are illustrated in Figure 2. These spectra highlighted qualitatively the same set of minerals grouped into major (M), minor (m) and trace (tr) minerals (Table 1). As mentioned, the majority minerals identified according to their relative abundance and XRD angles were lizardite and antigorite ($2\theta \approx 41.6$ & 14.7°), and to a lesser extent, chrysotile. Distinction of relative abundances of the three serpentine polymorphs, i.e., lizardite, antigorite and chrysotile, as a function of four sieved fractions was not attempted because of limitations of the field XRD analyzer at our disposal. However, considering the origin of the tailings chrysotile is expected to be the minor polymorph. Moreover, the specific surface area tended to increase as the size fractions became finer (Table 1). Doubling of the specific surface area from (+1580) to (+150) μm fractions (Table 1) could partly be ascribed to a tendency for the chrysotile fibers to accumulate preferentially towards the finer fractions as well as reduction in particle size. Furthermore, hydromagnesite ($2\theta \approx 38.1°$), magnetite and talc belonged to the minority minerals in addition to traces of iron-containing clinochlore and biotite found across all the size fractions. These spectra also reveal that the intensity of the peak assigned to hydromagnesite increased while moving from the coarser to the finer size fraction in accordance with a similar increasing trend of the samples carbon grade (Table 1).

Samples from the four particle size classes were also studied by means of Raman spectroscopy (Figure 3) with Raman spectra and corresponding photo insets: (1) = (+1580) μm (Figure 3-(1)); (2) = (+600) μm (Figure 3-(2)); (3) = (+300) μm (Figure 3-(3)) and (4) = (+150) μm (Figure 3-(4)). Furthermore, Raman spectra for reference minerals of predominantly single-polymorph chrysotile (a), lizardite (b), antigorite (c) as well as talc (d) (see photo insets in Figure 3) were also acquired to help discriminating the serpentine polymorphs contained in the sieved tailings. In agreement with the literature (O'Hanley and Wicks 1995;

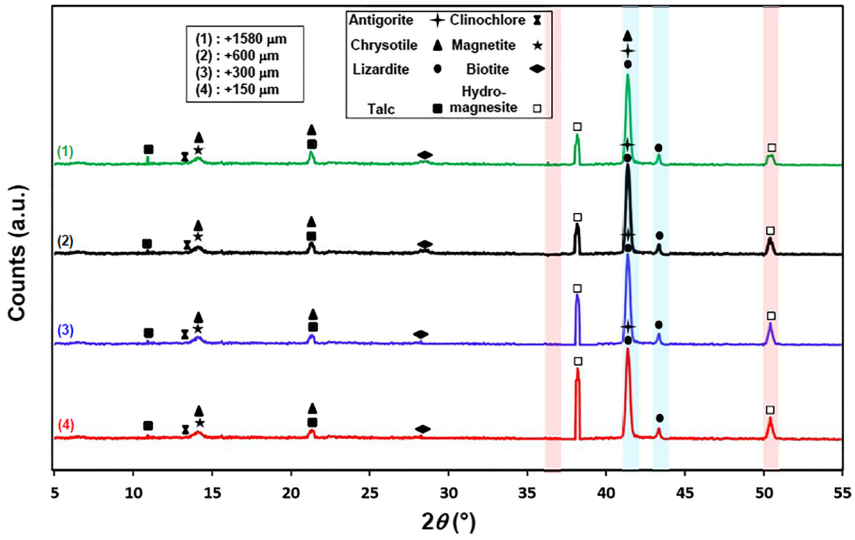

Figure 2: XRD spectra corresponding to samples from each sieved fraction of the mining residue.

Sarvaramini and Larachi 2011), the small band emerging at the highest wavenumber near 1100 cm^{-1} is typical of antisymmetric stretching mode of the Si–O_{nb} groups associated with chrysotile (Figure 3a). In the same large-wavenumber region, a band is also visible in the case of lizardite (Figure 3b) which was assigned to vibrations of the SiO_4 tetrahedra or silicon-oxygen bonds linkages according to Rinaudo and Gastaldi (O'Hanley and Wicks 1995). Antigorite is relatively inactive over this same wavenumber region with an inchoate protrusion (Figure 3c) possibly assigned to antisymmetric stretching modes of the Si–O_b–Si (Groppo et al. 2006; Kloprogge and Frost 1999; Rinaudo and Gastaldi 2003). The band protruding around 690 cm^{-1} is a signature of the symmetric stretching mode of the Si–O_b–Si groups (Figure 3a–c). Being common to the three serpentine polymorphs, it cannot be used for discrimination (Groppo et al. 2006; Kloprogge and Frost 1999; Rinaudo and Gastaldi 2003; Sarvaramini and Larachi 2011). The lower-intensity band detected at 627 cm^{-1} for all three serpentine polymorphs (Figure 3a–c) is reminiscent of the OH–Mg–OH translation modes (O'Hanley and Wicks 1995), and likewise would barely be helpful in discerning among the three magnesium silicates. Moreover, two bands are visible in the Raman spectrum at 390 and 349 cm^{-1}. For all three polymorphs, the higher-intensity band is assigned to bending vibrations of the SiO_4 tetrahedra (Groppo et al. 2006; Kloprogge and Frost 1999; O'Hanley and Wicks 1995; Rinaudo and Gastaldi 2003; Sarvaramini and Larachi 2011). Also, the band lying at 235 cm^{-1} is attributed to vibrational features stemming from the O_{nb}–H–O groups which involve one silicate non-bridging oxygen atom and a hydroxyl group from a nearby Mg–OH moiety. Its commonness to lizardite, antigorite and chrysotile makes it non-specific marker for discrimination. Interestingly, antigorite lack of vibrational activity nearby 543 and 462 cm^{-1} could make this region worthy of further inspection for discriminating which form of polymorph is contained in the tailings sieved fractions. Finally, in comparison to the serpentine vibrational features, the Raman spectrum of talc over the 1100– 200 cm^{-1} range purports relatively fewer features, especially a prominent band at 678 cm^{-1} and a tepid vibrational activity near 368 cm^{-1} (Figure 3d).

Visual inspection of Raman spectra for these reference minerals along with the spectra acquired for each sieved fraction (Figure 3-(1)–(4)) shows that most of the single-mineral vibrational bands are also borne in the sieved multi-mineral (Figure 2) fractions. The tendency to broadening of the bands in the latter spectra went up with coarsening of the sieved fractions. Such broadening was also accompanied with a drift in the positions of the main bands towards the lower (687 *vs.* 690 cm^{-1}, 379 *vs.* 390 cm^{-1} and 229 *vs.* 235 cm^{-1}) or higher wavenumbers (1110 *vs.* 1100 cm^{-1}) as is especially perceivable for the coarsest fraction. In the region near 627 cm^{-1}, the brucite-like sheets present in the tri-octahedral layers of the hydrous phyllosilicate structures (Larachi, Daldoul, and Beaudoin 2010) contribute with a lower-intensity signal as ascertained from the single-mineral Raman spectra. Interestingly, strengthening of the 627 cm^{-1} band, irrespective of sieved fractions, could be attributed to the presence of unreacted native brucite (Assima et al. 2014) though its detection through XRD was unresolved. The band intensities of the vibration modes at 543 and 462 cm^{-1} tended to slightly fade out from the coarser towards the finer fractions. These signatures are prominent in the Raman spectrum of the single-mineral lizardite sample (Figure 3b). This possibly suggests that the relative proportion among the

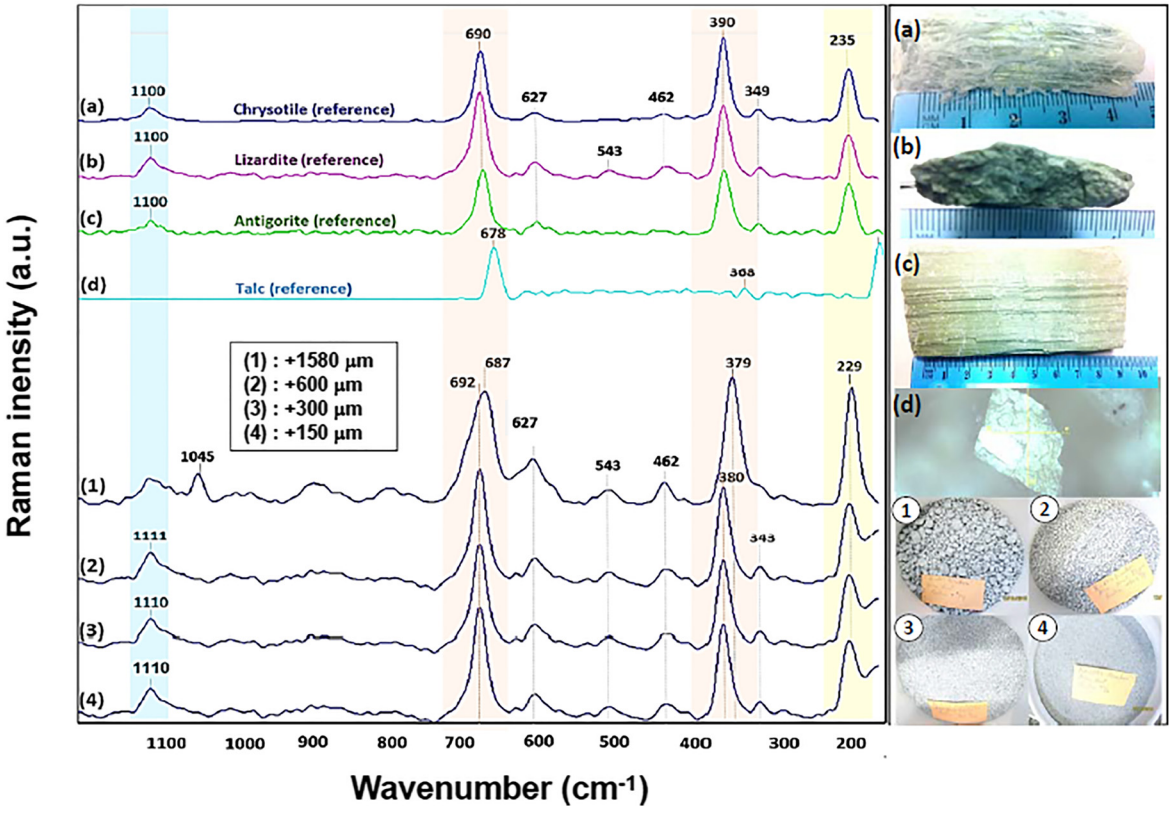

Figure 3: Raman spectra corresponding to each sieved fraction: (a)–(d) indicating spectra of reference minerals and their corresponding photos, and also (1)–(4) indicating spectra of mining sample residue in four selected fraction sizes and their corresponding photos.

serpentine polymorphs is inhomogeneous from one fraction to another. Likewise, it can be concluded that chrysotile has tendency to accumulate (as short fibers) in the finest fraction in accordance with above surface area observations. Peaks at 543 and 462 cm^{-1} go undetected in the case of antigorite alone (Figure 3c). However, it is not the reason to exclude the presence of antigorite in the sieved fractions, because of the lizardite and chrysotile interfering Raman vibrational features. Therefore, it can be concluded from Raman studies that lizardite would be a predominant polymorph whereas chrysotile would be present in minor quantities.

3.2 Hydrocyclone separation

This part of study endeavors to identify operating conditions favorable to beneficiate lizardite/antigorite (by hydrocyclone) at the expense of magnetite and fibrous chrysotile (both considered as contaminants in the separated product stream).

Recoveries are reported in terms of Fe (Figure 4a), Si (Figure 4b), and Mg (Figure 4c) for the hydrocyclone UFH-2 concentrate (as final product of hydrocycloning) as a function of the sieved fraction (+1580, +600, +300 and +150 µm) and for different concentrations of solids in the pulp. Irrespective of the treated fraction, an increase in solids pulp concentration tended to decrease the quality of UFH-2 concentrate (Figure 1) in terms of iron contamination (Figure 4a). For instance, virtually all the iron contained in the finest fraction was retained in the concentrate (Figure 4a) suggesting that, regardless of pulp loading, density differences amongst minerals did not promote sizable entrainment of magnetite particles into OFH-1 and OFH-2 overflow streams. The tendency to cut on iron contamination was more favorable for the coarsest size fraction especially at the lowest pulp concentration (Figure 4a). Although this was tantamount to lesser Si and Mg recoveries (Figure 4a,b), the decreasing iron grade from 7.47% (+150 µm class) to 5.15% (+1580 µm class) leans towards privileging treatment of the coarsest sieved fraction (Table 1).

The Si/Mg and Fe/Si ratios of hydrocyclone products at different pulp solids concentrations are shown in Figure 5a–d, respectively. During the process of concentrating lizardite and antigorite by hydrocycloning, variations (increase or decrease) in the levels of Mg, Si, and Fe as the major elements in the concentrates were observed and given in Table 2. The dashed line in Figure 5a,b represent

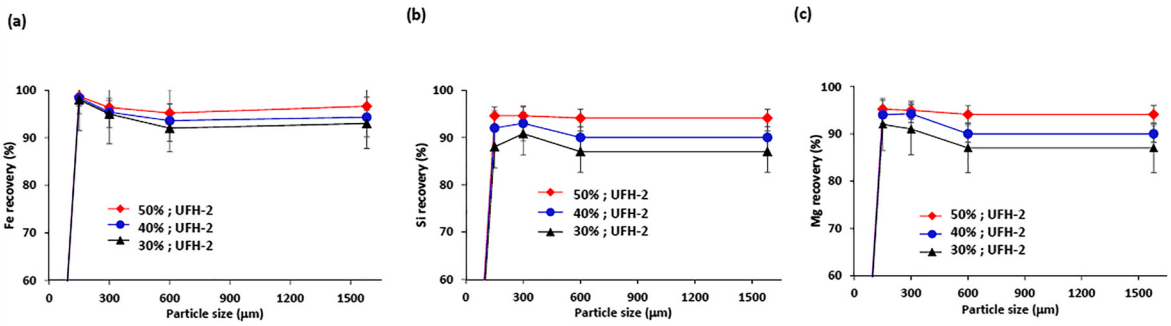

Figure 4: Recovery trends of (a) Fe, (b) Si and (c) Mg for the hydrocyclone UFH-2 concentrate at different size fractions.

the theoretical Si/Mg ratio for iron-free serpentines. The standard deviations between the results obtained are due to the instability of the hydrocyclone feed pump, sampling and dilutions which did not allow a sufficiently coherent material balance to be obtained.

For a given pulp concentration, the concentrate Si/Mg ratios tended to decrease as the treated size fraction became finer (Figure 5a). This was accompanied with a nearly monotonic increase of the Fe/Si ratio (Figure 5c) of the corresponding concentrates.

In this study, for the concentrates recovered from the underflow, the Si/Mg ratios at 30% solids show Si/Mg ratios greater than 0.67 (Si/Mg ≈ 0.77 and 0.78) (Figure 5a), with Fe/Si variations between 0.25 and 0.35 (Figure 5c). Si/Mg ratio = 0.67 is interpreted to correspond to lizardite in which iron is present in the crystal structure (O'Hanley and Wicks 1995). Likewise, Si/Mg ratio of 0.78 indicates chrysotile containing about 49.2% iron in the crystal lattice (Sarvaramini and Larachi 2011). Therefore, it can be concluded that these concentrates possibly contain iron-rich silicates, quartz (SiO_2) probably combined with an amorphous material potentially undetected in XRD. Conversely, the overflow Si/Mg ratios are almost equal to chrysotile theoretical ratio (Si/Mg ≈ 0.78), (Figure 5b) with low Fe/Si ratios of 0.05–0.25 (Figure 5d).

On the other hand, the Si/Mg ratio exceeded the 0.77 theoretical limit (Figure 5a,b) for the concentrate and overflow alike, and the hydrocyclone-treated sieved fraction. However, Si prevailed mostly in the serpentine minerals as shown from the XRD-identified crystalline species (Figure 2). The presence of talc and biotite would unlikely be responsible for such inflated Si/Mg ratios. A more plausible interpretation for these ratios is rather attributable to iron incorporation into the serpentine lattice and

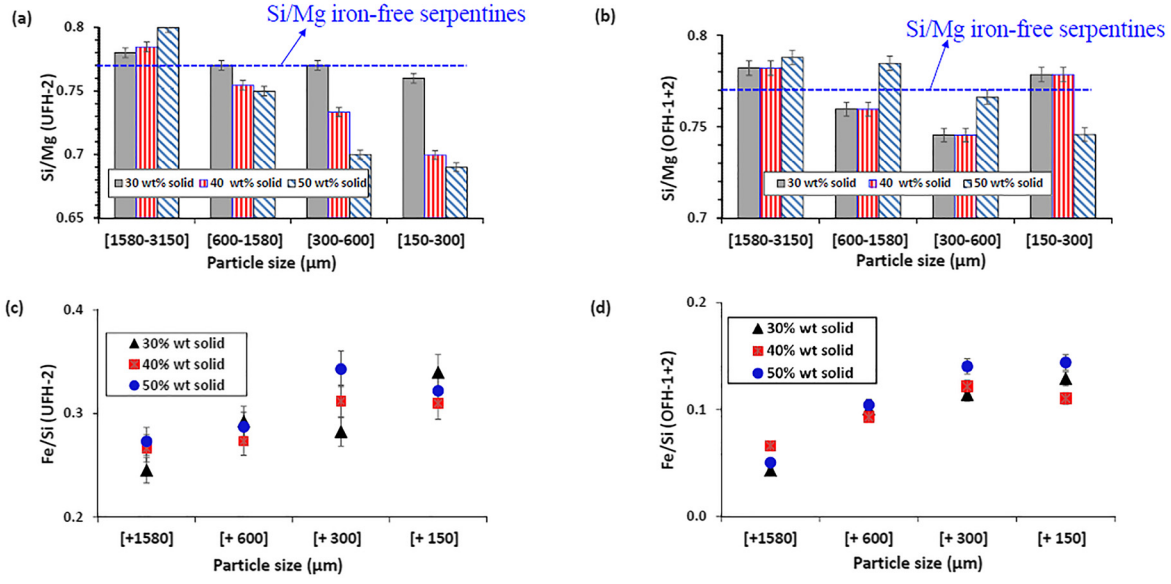

Figure 5: Dependence of Si/Mg (a, b) and Fe/Si (c, d) mass ratios to particle size and pulp concentration for underflow stream (UFH-2) concentrate and compounded overflow streams (OFH-1+2).

Table 2: Si, Fe & Mg recoveries after hydrocyclone separation for the concentration of lizardite/antigorite.

Pulp solid percent	Elements	Recovery of elements (%) in different sieved fraction (µm)			
		(+1580)	(+600)	(+300)	(+150)
30%	Si	88.1 (±1.6)	86.5 (±1.3)	90.8 (±2.1)	86.9 (±1.1)
	Mg	87.4 (±1.8)	87.2 (±1.1)	91.9 (±1.3)	92.6 (±1.3)
	Fe	93.1 (±0.9)	92.2 (±0.8)	95.3 (±0.9)	98.1 (±0.8)
40%	Si	90.1 (±1.3)	90.6 (±1.1)	93.1 (±1.1)	92.3 (±1.3)
	Mg	91.2 (±1.6)	92.1 (±0.9)	94.2 (±0.7)	94.0 (±0.3)
	Fe	94.3 (±1.1)	93.6 (±1.3)	95.4 (±1.4)	98.4 (±0.8)
50%	Si	94.5 (±1.3)	94.1 (±0.3)	94.6 (±1.3)	94.6 (±1.0)
	Mg	94.2 (±1.1)	93.9 (±0.8)	94.9 (±1.4)	95.2 (±1.3)
	Fe	96.7 (±1.2)	95.2 (±1.4)	96.4 (±1.2)	98.7 (±1.2)

substitution with Mg during the underground hydrothermal processes leading to these ultramafic rocks (Büttner and Saager 1982).

Regarding the solid percent effect, at 30% solids percent, the final recoveries were 87.4% for Mg, 88.1% for Si and 93.1% for Fe, with Si/Mg and Fe/Si ratios of 0.78 (Figure 5a,c) and 0.25 (Figure 5c), respectively. For solid concentration values of 40 and 50%, the behavior of the hydrocyclone gradually changes from a classifier with an umbrella discharge (30% solids) to a thickener with a coil discharge (40 and 50% solids).

3.3 Efficiency of chrysotile fibers removal and SEM observations

SEM was also taken into account for further understanding of the separation process. Systematic SEM observations of the overflow (tailing) and underflow (concentrate) streams of the hydrocyclone for all the examined size fractions are illustrated in Figures 6 and 7. A key observation arises from

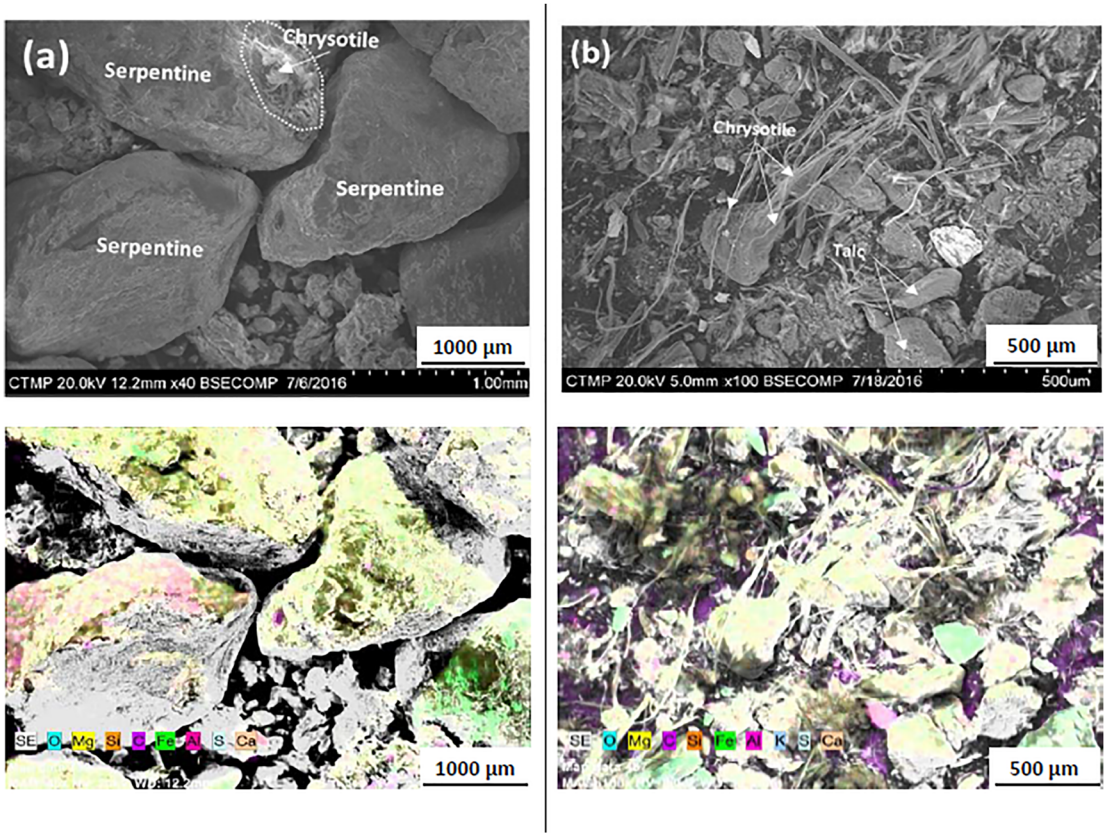

Figure 6: SEM images of hydrocyclone test for +1580 µm size class: (a) underflow (concentrate UFH-2) and (b) overflow (tailing OFH-2).

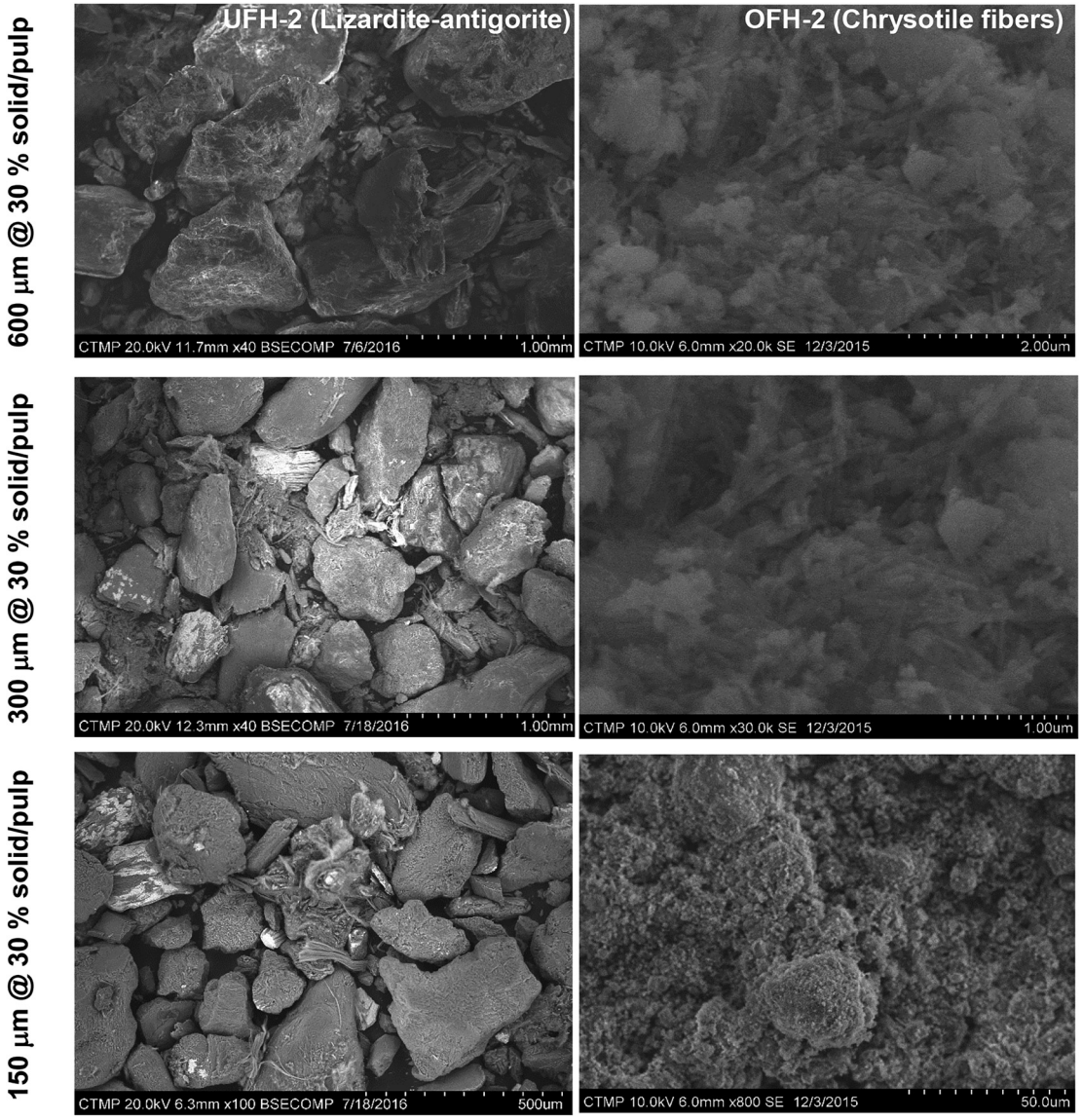

Figure 7: SEM images of underflow (UFH-2) & overflow (OFH-2) streams of 2nd hydrocyclone (see Figure 1) as a function of particle size fractions.

examination of the SEM images of the underflow (UFH-2) and overflow (OFH-2) streams of the second hydrocyclone as a function of particle size. Most of the fibrous structures are gotten rid of at the second hydrocyclone stage in the content of the underflow streams regardless of the tested size fraction. Nevertheless, the SEM photographs show some refractory fibers in UFH-2 streams but the contrast with the fluffy-looking overflow streams is staggering.

SEM images show the morphology and texture of the hydrocyclone products (Figure 6a,b). Plates in Figure 6a show the presence of large grains of serpentine minerals with low inclusions of chrysotile in the particle size class (+1580) microns for average ratios Si/Mg ≈ 0.78 and Fe/Si ≈ 0.25. On the other hand, plates in Figure 6b show a chrysotile fiber aggregate which consists of thin fibrils accompanied by talcum grains entrained in the overflow corresponding to Si/Mg ≈ 0.78, Fe/Si ≈ 0.05. Analysis of these figures shows that magnetite is mostly attached to the serpentine (Figure 6a) compared to the overflow (Figure 6b) where the observed Fe/Si ratios are almost nil. These semi-quantitative results indicate that chrysotile could successfully be separated into the overflow as reject of the separation process. However, the fine chrysotile fibrous entities, which still persist in the underflow concentrate (Figure 6a) will be subjected to further settling tests in a cascade of gravity separations to be discussed next.

3.4 Settling experiments

Settling tests were conducted only using hydrocyclone concentrates obtained from 30% solid percent concentration pulps. Indeed, this pulp composition was identified to correspond to the best conditions considering Fe content during hydrocyclone separation. The recoveries of Mg, Si and Fe in the underflow (concentrate) from the settling experiments carried out at different particle sizes are reported in Table 3. The objective of these laboratory-scale settling tests was to determine optimal operating conditions that could lead to the purification of the hydrocyclone concentrate (lizardite and antigorite) by deschlammation in order to extract the slurry or fine particles. It was observed that the recoveries in Mg and Si were almost constant in all the fraction sizes. While variations in recoveries of Fe (magnetite), as a contaminant, were observed. Optimal results were obtained for the +1580 µm size class sample where recoveries of 82.5 (±1.8) Mg, 82.6 (±0.8)% Si and 72.5 (±1.2) Fe (Table 3) were achieved.

The results of the influence of particle size on the settling kinetics as well as the monitoring of Si/Mg ratios are presented in Figure 8a–d, respectively. In the settling kinetic tests, optimal conditions were obtained in the cases of coarse fraction sizes (+1580 and +600 µm) due to the size and high density of these samples, as well as the low volume of chrysotile fiber in these size classes (Figure 8a). However, the settling kinetics observed for the finer particle size classes (+300 and +150 µm) indicated a slowdown reduction in mass recovery yield which can be due to the formation of suspended fiber filaments, and hence developing hindered settling conditions.

Table 3: Mg, Si and Fe recoveries and mineralogical properties of the settling (underflow) concentrates as a function of particle size.

Pulp solid concentration	Elements	Recovery of elements (%) in various Fraction size (µm)			
		(+1580)	(+600)	(+300)	(+150)
5%	Si	82.6 (±0.8)	78.2 (±1.2)	70.5 (±0.7)	68.7 (±1.9)
	Mg	82.5 (±1.8)	77.1 (±2.1)	73.2 (±2.9)	70.8 (±3.1)
	Fe	72.5 (±1.2)	71.2 (±0.9)	73.1 (±1.3)	67.8 (±3.3)
Identified minerals by XRD		**(+1580)**	**(+600)**	**(+300)**	**(+150)**
Lizardite [Mg_3 ($Si_{2-x}0_5$) (OH) $_{4-4x}$]		M	M	M	M
Antigorite [Mg_3 ($Si_{2-x}0_5$) (OH) $_{4-4x}$]		M	M	M	M
Chrysotile [Mg_3 ($Si_{2-x}0_5$) (OH) $_{4-4x}$]		m	m	m	m
Magnesite [$Mg(CO_3)_4(OH)_2{\cdot}4H_2O$]		m	m	m	m
Magnetite [($Fe^{2+}Fe_2^{3+}$) O_4]		m	m	m	m
Talc [Mg_3 ($Si0_5$)$_2$(OH)$_2$]		m	m	m	m
Clinochlore[(Mg, Fe^{2+})$_5$Al(Si_3Al) $O_{10}(OH)_8$]		tr	tr	tr	tr
Biotite [$KMg_3AlSi_3O_{10}(OH)F$]		tr	tr	tr	tr

M = major (10%); m = minor (1%); tr = trace (less than 1%).

In the cases of coarse fractions, mass recoveries ranged from 80 to 83% with Si/Mg ratios ≈0.78 during the first 20 min (Figure 8a). Note that these ratios exceed the Si/Mg ratio of theoretical lizardite (Si/Mg ≈ 0.67) (Fouquet et al. 1997). Also, Figure 8b shows that the mass recoveries of the overflow decreased during time with computed Si/Mg ratios around 0.78 (Figure 8d) and corresponding theoretically to those of chrysotile (Büttner and Saager 1982). Conversely, for the fine fractions, the recoveries of underflow varied between 69 and 71% over the first 20 min (Figure 8a) with Si/Mg ratios around 0.78 (Figure 8c) which are also higher than lizardite Si/Mg theoretical ratio. This higher value of Si/Mg ratio of the concentrates can be ascribed to the presence of various minerals such as magnetite, iron-rich silicates as well as quartz combined with a potentially undetected amorphous silicate. In the overflow, the Si/Mg ratios obtained for these fine fractions are lower than those anticipated on the basis of chrysotile theoretical stoichiometry (Büttner and Saager 1982).

SEM was also used to analyze overflow and underflow samples to disclose further information regarding the separation. A key observation arises from examination of the SEM images of the underflow (UFS-6) and overflow (OFS-6) streams of the last decantation unit as a function of particle size. Chrysotile fibers in the underflow streams after six decantation operations of the UFH-2 stream are virtually undetectable in UFS-6 in the case of the coarsest fraction (Figure 9a). However, one can see that very few fiber leftovers may be present in the underflow stream the finer the treated particle size fraction (Figure 10). Therefore, a focus on valorizing the coarsest fractions should be the safest among all the sieved fractions according to our SEM analyses.

The SEM images show the morphology and texture of the decantation products (Figure 9). These photographs show the qualitative aspect of the decantation products obtained after 30 min at 5% solid percent in the pulp for particle size class +1580 µm. Figure 9a shows a photograph of a purified concentrate of lizardite and antigorite containing talc grains, ferromagnesian minerals, aluminosilicates and magnetite grains liberated and mostly in the form of inclusions. Conversely, plates indicated in Figure 9b show photographs of an agglomerate of chrysotile fibers accompanied by platelike grains (talc) and carbonates (e.g., magnesite) resulting from the capture of talc in the overflow. These semi-quantitative results demonstrate that chrysotile fibers can be more separated by settling experiments and the concentrate is relatively free of harmful fibers. This concentrate will be subjected to magnetic separation for further purification in the next step.

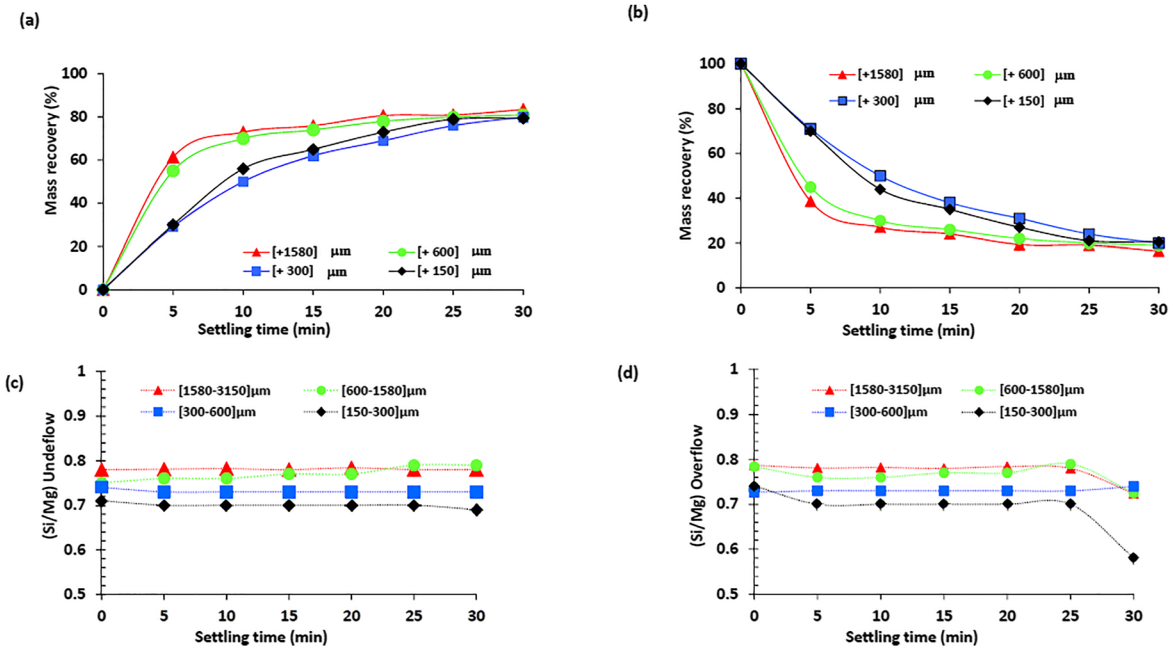

Figure 8: Influence of particle size on the settling kinetics in terms of: (a) underflow mass recovery, (b) overflow mass recovery, (c) evolution of Si/Mg in underflow and (d) evolution of Si/Mg in overflow.

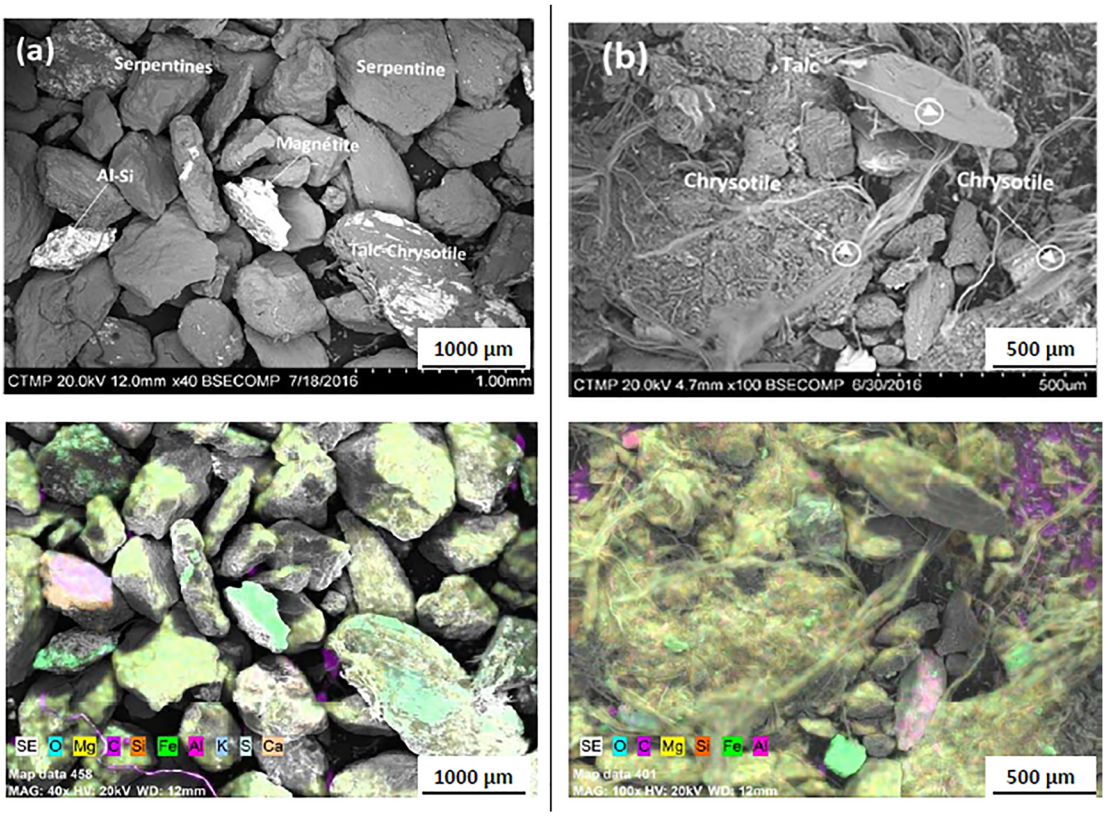

Figure 9: SEM images of settling test for +1580 µm size class: (a) underflow and (b) overflow.

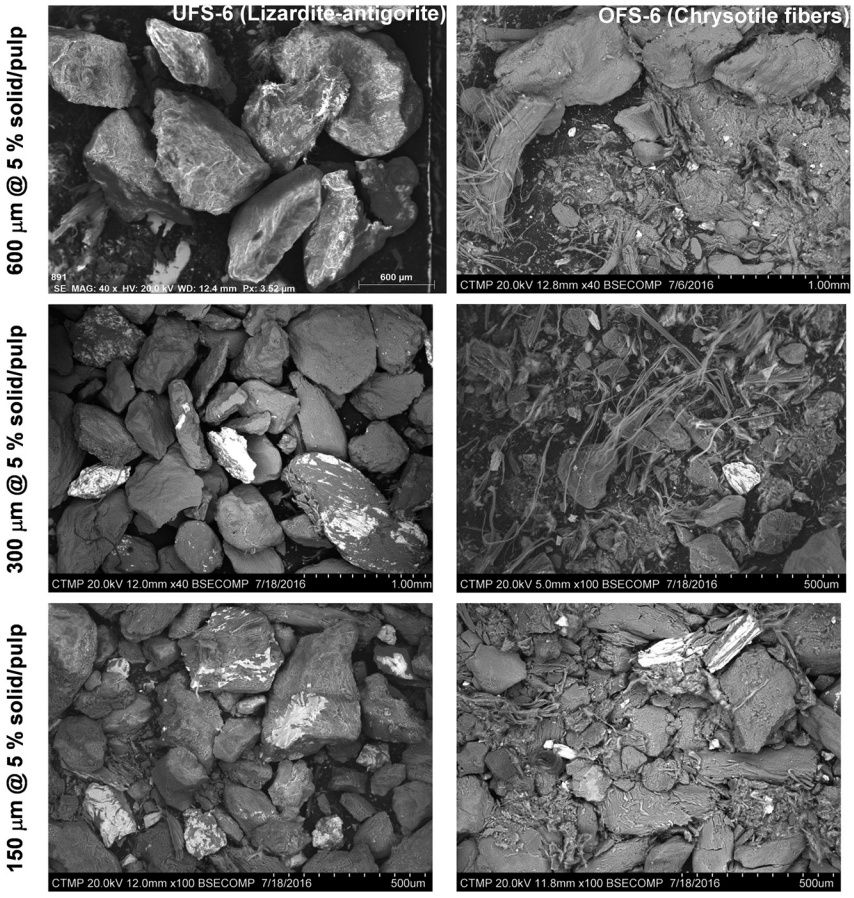

Figure 10: SEM images of underflow (UFS-6) & overflow (OFS-6) streams of 6th decantation unit (Figure 1) as a function of particle size fractions.

3.5 Magnetic separation

Si, Mg and Fe recoveries from the non-magnetic fractions at the second pass of the magnetic separator obtained on the settling concentrates are shown in Table 4.

Optimal conditions for magnetic separation were obtained at a magnetic intensity of 700 Gauß on the dried settling concentrates with +1580 μm size class. The mass percentage of the non-magnetic fraction was 65.0% (±1.8) with a recovery efficiency of 62.5% (±0.9) for Mg recovered from the raw feed. The resulting concentrate contains 56.5% iron included in lizardite and antigorite. X-ray diffractograms of the raw samples and non-magnetic concentrates for different Si/Mg ratios are shown in Figure 11.

Table 4: Mg, Si and Fe recoveries and properties of non-magnetic concentrates as a function of particle size.

Magnetic intensity	**Elements**	**Recovery of elements (%) in various size fraction (μm)**			
		(+1580)	**(+600)**	**(+300)**	**(+150)**
700 Gauß	Si	14.1(±1.6)	54.1(±0.6)	55.0(±0.8)	49.1(±0.6)
	Mg	62.5(±0.9)	55.5(±0.9)	54.5(±0.6)	48.9(±1.1)
	Fe	56.5(±0.8)	22.1(±0.8)	15.7(±1.2)	9.11(±0.8)
Identified minerals by XRD		**(+1580)**	**(+600)**	**(+300)**	**(+150)**
Lizardite [Mg_3 ($Si_{2-x}0_5$) (OH) $_{4-4x}$]		M	M	M	M
Antigorite [Mg_3 ($Si_{2-x}0_5$) (OH) $_{4-4x}$]		M	M	M	M
Chrysotile [Mg_3 ($Si_{2-x}0_5$) (OH) $_{4-4x}$]		m	m	m	m
Magnesite [$Mg(CO_3)_4(OH)_2{\cdot}4H_2O$]		m	m	m	m
Magnetite [($Fe^{2+}Fe_2^{3+}$) O_4]		m	m	m	m
Talc [Mg_3 ($Si0_5$)$_2$(OH)$_2$]		m	m	m	m
Clinochlore[(Mg, Fe^{2+})$_5$Al(Si_3Al)$O_{10}(OH)_8$]		tr	tr	tr	tr
Biotite [$KMg_3AlSi_3O_{10}(OH)F$]		tr	tr	tr	tr

M = major (10%); m = minor (1%); tr = trace (less than 1%).

The main crystal phases observed for the non-magnetic concentrates, identified successively as C1, C2, C3 and C4 in the figure, were assigned to lizardite and antigorite.

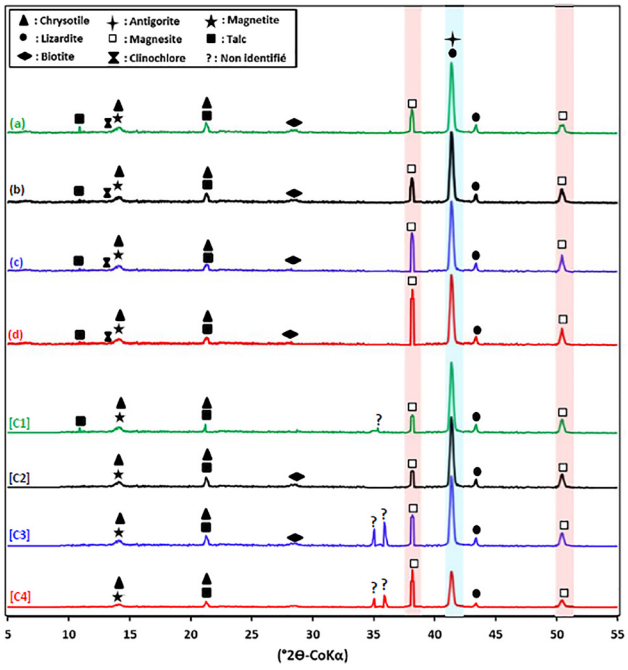

Figure 11: X-ray diffraction spectra of the sieved mining residue: (a) +1580 µm, (b) +600 µm, (c) +300 µm and (d) +150 µm and also for the non-magnetic concentrates C1–C4 (Data acquired using Co line Kα over a diffraction angle of 2 θ ranging from 5 to 55°).

Magnetite and magnesite were also found in the concentrate. Other crystal phases detected were minor and included biotite, clinochlore, talc, and other unidentified phases. The obtained spectra show a strong presence of magnesite in the fine particle size classes (+300 and +150 µm) with high X-ray intensities and a weak presence in the coarse ones (+1580 and +600 µm). The Fe/Si ratios were around 0.1. These results confirm that these fractions are controlled by magnesite and magnetite and possibly by other unidentified mineral phases.

The ratios of Si/Mg and Fe/Si of the non-magnetic and magnetic concentrates are shown in Figure 12a–d, respectively. Variations (increase or decrease) in Mg, Si and Fe contents as the main elements in concentrates were observed in the magnetic and non-magnetic fractions. Table 4 summarizes the analyses in terms of Mg, Si and Fe recoveries and mineralogical properties of non-magnetic concentrates as a function of particle size. The Si/Mg ratio was chosen as the main indicator of the separation efficiency in comparison with theoretical Si/Mg ratio of lizardite and antigorite (Figure 12a,b). Likewise, the Fe/Si ratio was chosen as a secondary indicator for the presence of iron with(in) the serpentine rock (Figure 12c,d). Concerning the non-magnetic fractions, the Si/Mg ratios for the coarse grain size classes (+1580 and +600 µm) were slightly higher than the theoretical ratio for lizardite (0.67 [Fouquet et al. 1997]) (Figure 12a) with Fe/Si ratios equal to 0.15 and 0.10 (Figure 12c). On the contrary, for the non-magnetic fractions corresponding to the fine grain size classes, the Si/Mg ratios were less than 0.67

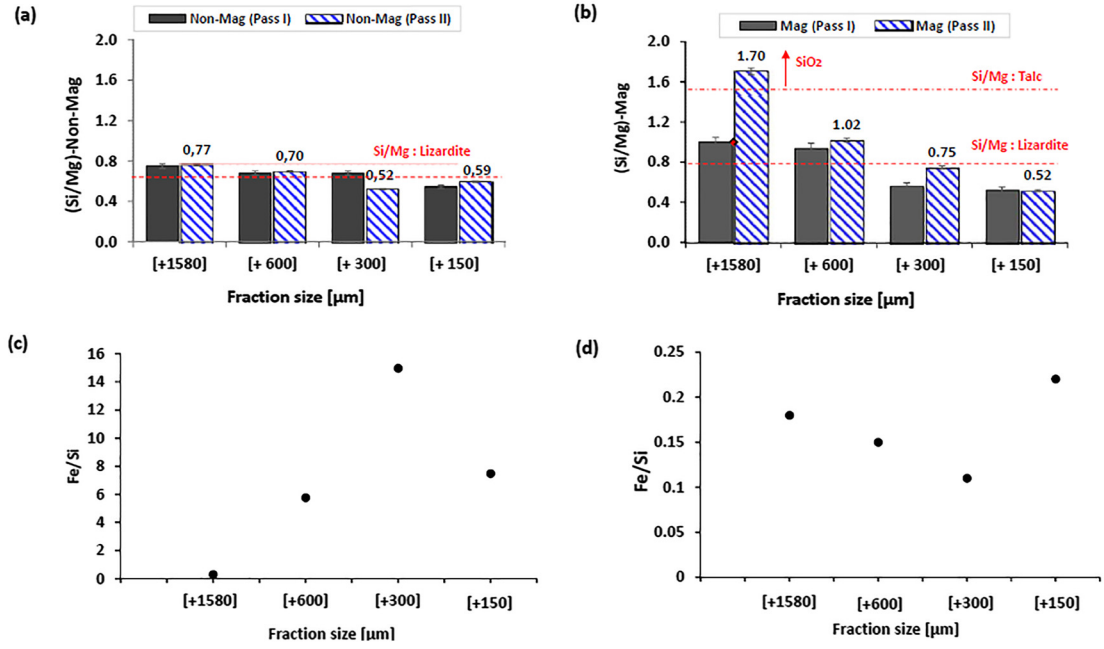

Figure 12: Si/Mg ratio of (a) non-magnetic and (b) magnetic concentrates, and of Fe/Si ratio for (c) non-magnetic and (d) magnetic concentrates.

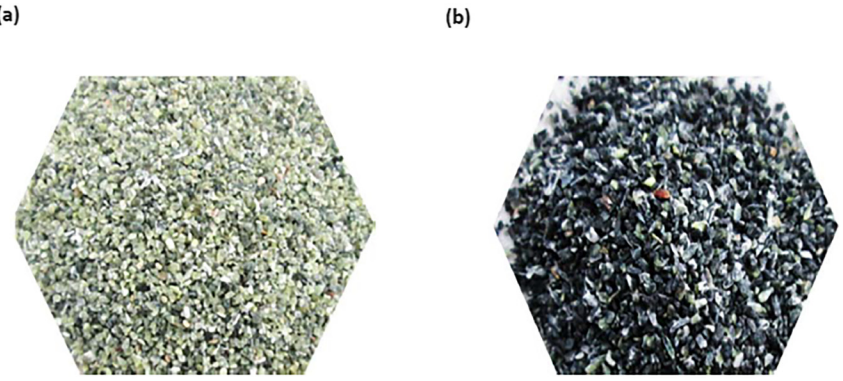

Figure 13: Photographs of magnetic separation products: (a) non-magnetic fraction and (b) magnetic fraction.

(Fouquet et al. 1997). This suggests that these concentrates are mostly controlled by carbonates and mainly magnesite observed in XRD (Figure 11) as compared to the coarse fractions. The magnetic fractions (Figure 12b,d) contain more iron (magnetite) than carbonates at low levels. Figure 12b reveals an excessive entrainment of talc and quartz at the second pass of the magnet in non-magnetic concentrates (lizardite and antigorite). The latter possibly containing iron-rich silicates, and quartz (SiO_2) probably combined with a potentially amorphous phases undetected by XRD.

Figures 11b and 13a help grasp an optical overview of the products from the magnetic separation for the +1580 µm fraction in the case of non-magnetic and magnetic fractions, respectively. Differences in their colors provide an additional qualitative assessment of the separation between magnetic and non-magnetic minerals through the chain of separation units examined in this study.

4 Conclusion

Beneficiation of lizardite and antigorite concentrate from a serpentine rock mining residue through physical separators was studied in order to identify some optimal parameters at each stage of the separation process. For this purpose, three physical separation techniques consisting of hydrocycloning, decanting (settling) and magnetic separation were undertaken for four size classes of the residue, namely (−3150, +1580), (−1580, +600), (−600, +300) and (−300, +150) µm. Hydrocycloning, as the most economical method for beneficiation of lizardite and antigorite, was firstly taken into consideration. A recovery of 85% (±4) in magnesium (Mg) was achieved for the particle size class +1580 µm. Underflow of two steps hydrocycloning was used for settling experiments for further processing. Settling tests lasting 30 min led to recoveries of 82.5% (±1.8) of Mg in a purified concentrate. Then, after six settling steps, the final underflow was routed to a magnetic separation unit in which two steps of magnetic separation were carried out. Magnetic separation in two steps produced a final non-magnetic concentrate with a recovery of 62.5% (±0.9) wt. of Mg with low iron content. SEM characterizations revealed that it was possible to reduce substantially the amount of chrysotile fibers to render the coarse-sized fraction in the mining waste usable while significantly lowering the health risk of the fibers. This nearly non-magnetic concentrate of lizardite and antigorite can be contemplated as a purified feed stream for chemical or biological leaching for Mg extraction as well.

Acknowledgments: One of the authors (DK) acknowledges the Scholarship program "*Bourse en milieu pratique BMP Innovation* (FRQNT-CRSNG-CTMP Thetford Mines)".
Author contributions: All the authors have accepted responsibility for the entire content of this submitted manuscript and approved submission.
Research funding: This study was funded by FRQNT-CRSNG-CTMP Thetford Mines.
Conflict of interest statement: The authors declare no conflicts of interest regarding this article.

References

Assima, G. P., F. Larachi, J. Molson, and G. Beaudoin. 2014. "Comparative Study of Five Québec Ultramafic Mining Residues for Use in Direct Ambient Carbon Dioxide Mineral Sequestration." *Chemical Engineering Journal* 245: 56–64.

Barbeau, C., S. Couture, and J. C. Roy. 1972. "Composition of the Asbestos Tailings from the Mines in the Eastern Townships of Québec – Industrial Minerals from Waste." *Canadian Mining and Metallurgical Bulletin* 65: 51–2.

Blazy, P. 1970. *La valorisation des minerais*, 416. Paris: Presses Universitaires de France.

Bodénan, F., F. Bourgeois, C. Petiot, T. Augé, B. Bonfils, C. Julcour-Lebigue, F. Guyot, A. Boukary, J. Tremosa, A. Lassin, E. C. Gaucher, and P. Chiquet. 2014. "Ex Situ Mineral Carbonation for CO2 Mitigation: Evaluation of Mining Waste Resources, Aqueous Carbonation Processability and Life Cycle Assessment (Carmex Project)." *Minerals Engineering* 59: 52–63.

Büttner, W., and R. Saager. 1982. "Rapid XRD Determination of the Chrysotile/Lizardite Ratios in Asbestos-Bearing Serpentines." *Tschermaks mineralogische und petrographische Mitteilungen* 30: 177–87.

Case, B. W., A. Churg, A. Dufresne, P. Sebastien, A. McDonald, and J. C. McDonald. 1997. "Lung Fibre Content for Mesothelioma in the 1891–1920 Birth Cohort of Quebec Chrysotile Workers: a Descriptive Study." *Annals of Occupational Hygiene* 41: 231–6.

Collings, R. K. 1977. *Mineral Waste Resources of Canada: Report No. 2, Mining Wastes in Québec*. Ottawa: CANMET.

Evans, B. W. 2010. "Lizardite versus Antigorite Serpentinite: Magnetite, Hydrogen, and Life (?)." *Geology* 38: 879–82.

Fouquet, Y., J.-L. Charlou, H. Ondréas, J. Radford-Knoery, J.-P. Donval, E. Douville, R. Apprioual, P. Cambon, H. Pellé, J.-Y. Landuré, A. Normand, E. Ponsevera, C. German, L. Parson, F. Barriga, I. Costa, J. Relvas, and A. Ribeiro. 1997. "Discovery and First Submersible Investigations on the Rainbow Hydrothermal Field on the MAR (36°14 N)." *Eos Transactions of American Geophysical Union* 78 (46): 832–40.

Germine, M., and J. H. Puffer. 2015. "Analytical Transmission Electron Microscopy of Amphibole Fibers from the Lungs of Quebec Miners." *Archives of Environmental & Occupational Health* 70: 323–31.

Germine, M., and J. H. Puffer. 2020. "Tremolite–actinolite Fiber Coatings of Sub-nanometer Silica-Rich Particles in Lungs from Deceased Quebec Miners." *Toxicology and Industrial Health* 36: 146–52.

Groppo, C., C. Rinaudo, S. Cairo, D. Gastaldi, and R. Compagnoni. 2006. "Micro-Raman Spectroscopy for a Quick and Reliable Identification of Serpentine Minerals from Ultramafics." *European Journal of Mineralogy* 18: 319–29.

Hamilton, J. L., S. A. Wilson, B. Morgan, C. C. Turvey, D. J. Paterson, S. M. Jowitt, J. McCutcheon, and G. Southam. 2018. "Fate of Transition Metals during Passive Carbonation of Ultramafic Mine Tailings via Air Capture with Potential for Metal Resource Recovery." *International Journal of Greenhouse Gas Control* 71: 155–67.

Hébert, Y. 1985. *Géologie des gîtes et indices de talc de la région de Thetford Mines (MB 85-38)*, 1–49. Québec: Gouvernement du Québec, Ministère de l'Énergie et des Ressources.

Huot, B. G., and R. Hébert. 2003. *Le piégeage du CO_2 anthropique dans les parcs à résidus d'amiante du sud du Québec: concept et valorisation, rapport final du projet séquestration du CO_2*, 52–4. Québec: Université Laval.

Kloprogge, J. T., and R. L. Frost. 1999. "Fourier Transform Infrared and Raman Spectroscopic Study of the Local Structure of Mg-, Ni-, and Co Hydrotalcites." *Journal of Solid State Chemistry* 146: 506–15.

Larachi, F., I. Daldoul, and G. Beaudoin. 2010. "Fixation of CO_2 by Chrysotile in Low-Pressure Dry and Moist Carbonation – Ex-Situ and In-Situ Characterizations." *Geochimica et Cosmochimica Acta* 74: 3051–75.

Martinez, E. 1974. "New Method for Concentration of Asbestos Ore." *Transactions of the Society of Mining Engineers* 256: 86–8.

Mukherjee, A. K., R. Sripriya, P. V. T. Rao, and P. Das. 2003. "Effect of Increase in Feed Inlet Pressure on Feed Rate of Dense Media Cyclone." *International Journal of Mineral Processing* 69: 259–74.

Neesse, T., M. Schneider, V. Golyk, and H. Tiefel. 2004. "Measuring the Operating State of the Hydrocyclone." *Minerals Engineering* 17: 697–703.

Nicholson, W. J. 2001. "The Carcinogenicity of Chrysotile Asbestos – A Review." *Industrial Health* 39 (2): 57–64.

O'Hanley, D. S., and F. J. Wicks. 1995. "Conditions of Formations of Lizardite, Chrysotile and Antigorite, Cassiar, British Columbia." *The Canadian Mineralogist* 33 (4): 753–73.

Plitt, L. R., B. C. Flintoff, and T. J. Stuffco. 1987. "Roping in Hydrocyclone." In *Proceedings of the 3rd International Conference on Hydrocyclones, Oxford, England, 30 September–2 October*, 21–34. London, UK: Elsevier.

Rinaudo, C., and D. Gastaldi. 2003. "Characterisation of Chrysotile, Antigorite and Lizardite by FT-Raman Spectroscopy." *The Canadian Mineralogist* 41: 883–90.

Sztuke, J. 1979. "Recovery of Nickel and Iron Concentrates from the Asbestos Tailings of Carey Canada Inc." In *Third Conference of Open Pit Operator in the Thetford Mines*, Québec, Canada.

Riordon, P. H. 1973. *Geology of the Asbestos Deposits of Southeastern Québec (E.S. 18)*, 1–105. Ministère des Richesses Naturelles du Québec. Also available at http://gq.mines.gouv.qc.ca/documents/examine/dp186/DP186.pdf.

Sarvaramini, A., and F. Larachi. 2011. "Mössbauer Spectroscopy and Catalytic Reaction Studies of Chrysotile-Catalyzed Steam Reforming of Benzene." *Journal of Physical Chemistry C* 115: 6841–8.

Thibault, Y. 2011. Caractérisation minéralogique d'échantillons de surface de résidus miniers produits par l'extraction du chrysotile dans la région de Thetford Mines (Québec). Division Report. CANMET Mines. Also available at https://www.rncan.gc.ca/mines-materiaux/publications/14430

Veetil, S. P., G. Mercier, J. F. Blais, E. Cecchi, and S. Kentish. 2015. "Magnetic Separation of Serpentinite Mining Residue as a Precursor to Mineral Carbonation." *International Journal of Mineral Processing* 140: 19–25.

Viti, C., C. Collettini, T. Tesei, M. S. Tarling, and S. A. Smith. 2018. "Deformation Processes, Textural Evolution and Weakening in Retrograde Serpentinites." *Minerals* 8: 241–61.

Zarandi, A. E., F. Larachi, G. Beaudoin, B. Plante, and M. Sciortino. 2017. "Ambient Mineral Carbonation of Different Lithologies of Mafic to Ultramafic Mining Wastes/Tailings–A Comparative Study." *International journal of greenhouse gas control* 63: 392–400.